Passively *Q*-switched tri-wavelength Yb^{3+}:$GdAl_3(BO_3)_4$ solid-state laser with topological insulator Bi_2Te_3 as saturable absorber

Yi-Jian Sun,[1,2] Chao-Kuei Lee,[3] Jin-Long Xu,[1] Zhao-Jie Zhu,[1] Ye-Qing Wang,[4] Shu-Fang Gao,[1,2] Hou-Ping Xia,[1,2] Zhen-Yu You,[1] and Chao-Yang Tu[1,*]

[1]*Key Laboratory of Optoelectronic Materials Chemistry and Physics of CAS, Fujian Institute of Research on the Structure of Matter, CAS, Fuzhou, Fujian 350002, China*
[2]*University of Chinese Academy of Sciences, Beijing 100039, China*
[3]*Department of Photonics, National Sun Yat-sen University, Kaohsiung, Taiwan*
[4]*Department of Applied Physics, East China Jiaotong University, Nanchang, Jiangxi 330013, China*
**Corresponding author: tcy@fjirsm.ac.cn*

Received January 6, 2015; revised February 18, 2015; accepted March 4, 2015;
posted March 6, 2015 (Doc. ID 231768); published May 15, 2015

In this paper, we reported a multiwavelength passively *Q*-switched Yb^{3+}:$GdAl_3(BO_3)_4$ solid-state laser with topological insulator Bi_2Te_3 as a saturable absorber (SA) for the first time, to the best of our knowledge. Bi_2Te_3 nanosheets were prepared by the facile solvothermal method. The influence of three Bi_2Te_3 densities on the laser operation was compared. The maximum average output power was up to 57 mW with a pulse energy of 511.7 nJ. The shortest pulsewidth was measured to be 370 ns with 110 kHz pulse repetition rate and 40 mW average power. The laser operated at three wavelengths simultaneously at 1043.7, 1045.3, and 1046.2 nm, of which the frequency differences were within the terahertz wave band. Our work suggests that solvothermal synthesized Bi_2Te_3 is a promising SA for simultaneously multiwavelength laser operation.

OCIS codes: (140.3480) Lasers, diode-pumped; (140.3540) Lasers, Q-switched; (140.3580) Lasers, solid-state; (140.3615) Lasers, ytterbium.
http://dx.doi.org/10.1364/PRJ.3.000A97

1. INTRODUCTION

Simultaneously multiwavelength near-infrared pulsed lasers with high peak power and short pulse duration have widespread applications in nonlinear spectroscopy, free space optical communication, biomedicine, military, lidar, imaging holography, nonlinear optics, and the terahertz-wave difference frequency process [1–6]. The passively *Q*-switched solid-state laser is an efficient, reliable, and widely used technique to emit nanosecond level pulses. For such a laser, the saturable absorber (SA) is an element whose properties strongly determine the laser performance.

For decades, many successful *Q*-switched lasers have been realized by exploiting a variety of SAs such as transition-element-doped (Cr^{4+} [7,8], V^{3+} [9,10], and Co^{2+} [11]) host materials and semiconductor saturable absorber mirrors (SESAMs) [12–15]. However, it should be noted that the applications of these traditional SAs are somehow limited due to their narrow absorption band and high cost. In recent years, graphene, a 2D-structure layered carbon material with Dirac-like gapless electronic band structure, has garnered much attention for its absorption capacity [16–20] because of the intrinsic advantages such as broadband optical modulation, strong absorption, fast relaxation, and easy fabrication. The success of graphene draws researchers to investigate the photonic applications of other 2D materials. Similar to graphene, the topological insulators (TIs) are characterized by a linear dispersion band structure with the Dirac point. They have a narrow gap in the bulk state (0.2–0.3 eV) and a Dirac cone on the surface/edge [21], and both contribute to the saturable absorption [22,23]. In 2012, Bernard *et al.* first reported that TIs exhibit saturable absorption when placed in a 1550 nm laser beam [24]. Soon after, more detailed investigation into nonlinear optics and saturable absorption properties of TIs was carried out [25]. Recently, both mode-locked and *Q*-switched fiber lasers have been successfully realized with TI SAs [23,26–31]. However, the applications of TIs in solid-state lasers, which are more suitable for high-energy short pulse generation than fiber lasers due to having less nonlinear pulse-splitting, have not been addressed as much [32–35].

Laser gain material is the other key element for passively *Q*-switched lasers. The Yb ion has only two energy levels and weak electron–phonon coupling; therefore the excited state absorption effect, which strongly limits the laser efficiency in Nd^{3+} lasers, can be avoided in the Yb^{3+} counterpart. Furthermore, Yb ion's long upper-state lifetime (usually on millisecond order) induces strong energy storage and thus could be beneficial for high-energy pulse generation. The growth, spectroscopic, and Cr^{4+}:YAG passively *Q*-switched laser properties of a novel Yb^{3+} crystal, Yb^{3+}:$GdAl_3(BO_3)_4$ (Yb:GAB), were reported in our previous works [8,36,37]. It exhibits a broad emission band (~100 nm), which is beneficial for multiwavelength emission under laser optimization. Passive *Q*-switching of a Yb-doped fiber laser by few-layer TI Bi_2Se_3 has been successfully realized with yielding 1.95 μs pulses [26]. Recently a *Q*-switched Yb:KGW solid-state

laser with TI Bi_2Se_3 as a SA was realized with the shortest pulsewidth of 1.6 μs [35]. However, TIs have not been used to *Q*-switch Yb-doped nanosecond multiwavelength solid-state lasers to our best knowledge.

In this paper, we report on the investigation of a tri-wavelength *Q*-switched Yb:GAB solid-state laser with a Bi_2Te_3 TI as the SA. The Bi_2Te_3 sheets were synthesized by a facile solvothermal route. We prepared three TI SA samples with different density. The influence on the output power, pulsewidth, repetition rate, and emission wavelength was investigated in detail. This laser is suitable for various applications that require tunable laser and frequency mixing.

2. PREPARATION AND CHARACTERIZATION OF Bi_2Te_3 NANOSHEETS

Hexagonal Bi_2Te_3 single crystals with uniform morphology were synthesized by a facile solvothermal route the same as in Ref. [38]. All the chemicals used for the synthesis of the Bi_2Te_3 nanosheets in this work were analytical grade without further purification: 0.315 g of $BiCl_3$, 0.332 g of Na_2TeO_3, 0.4 g of NaOH, and 0.5 g of PVP were dissolved in 70 mL ethylene glycol (EG). After ultrasonication and stir for 20 min, the mixture solution was transferred into a 100 mL stainless steel autoclave. The autoclave was heated at 180°C for 36 h and then cooled to room temperature naturally. The gray powders were collected by centrifugation, washed by distilled water and ethanol several times, and finally dried at 60°C for 8 h.

The representative XRD spectrum in Fig. 1(a) shows the products of a pure rhombohedral phase of Bi_2Te_3 with a space group $R\bar{3}m$ (166), in good agreement with the standard card JCPDF #15-0863. Figure 1(b) gives the TEM image of the synthesized Bi_2Te_3, which shows a hexagon nanosheet with thickness of 30–50 nm. The flat surface and sharp edges indicate a homogeneous crystallinity. The bright diffraction spots in the SAED [inset in Fig. 1(b)] pattern also reveal the nanosheet to be a well-crystallized single crystal.

The modulation depth can be tuned in a wide range from 66.5% to 6.2% by varying the graphene thickness [39]. Thus three TI SA samples were prepared. The Bi_2Te_3 solution was dispersed in isopropyl alcohol solution by ultrasonicating Bi_2Te_3 nanosheets for 1 h. The concentration is ~0.23 mg/mL. Then we dropped the Bi_2Te_3 dispersion solution onto three 1 mm thick quartz substrates with 96% transmittance at around 1046 nm. With the increase of Bi_2Te_3 density on the substrate, we marked them TISA1, TISA2, and TISA3,

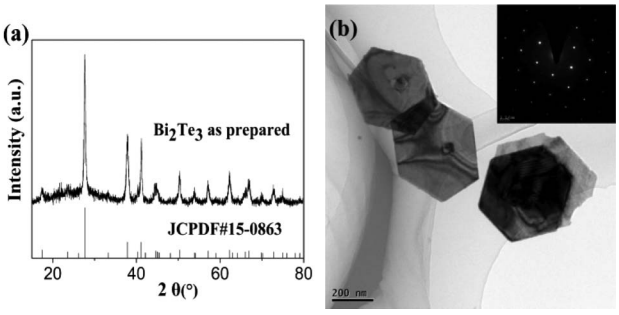

Fig. 1. (a) XRD diffraction pattern. (b) TEM image. Inset shows the corresponding SAED pattern of the as-grown Bi_2Te_3 nanosheets. The scale bar is 200 nm.

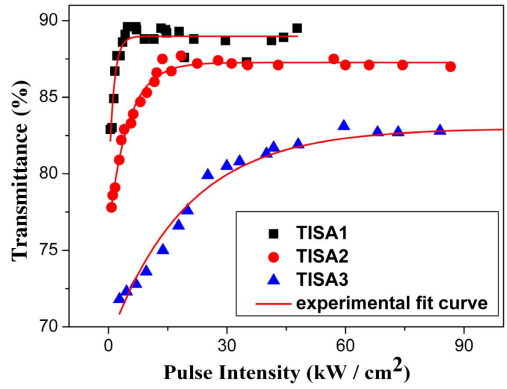

Fig. 2. Saturable absorption characteristic at 1.0 μm for three SA samples.

which are estimated to be 0.015, 0.031, and 0.054 mg/cm^2, respectively.

The optical saturable absorption properties were investigated by twin-detector measurement [34]. We used a home-made acousto-optic *Q*-switching solid-state laser at 1.0 μm as the laser source and detected the laser power before and after the TI samples to get the nonlinear transmission curve. The corresponding results of the three samples are shown in Fig. 2. By fitting the curve with the equation

$$T(I) = 1 - \Delta T * \exp(-I/I_{\text{sat}}) - T_{\text{ns}}, \quad (1)$$

where $T(I)$ is the transmittance, ΔT is the modulation depth, I is the input intensity, I_{sat} is the saturation intensity, and T_{ns} is the nonsaturable loss, the saturation intensity I_{sat} is extracted to be 1.26, 4.96, and 19.61 kW/cm^{-2}, and the modulation depth ΔT is 10.11%, 10.95%, and 13.96% for TISA1, TISA2, and TISA3, respectively. The saturation intensity is much lower than the previous reports measured by the Z-scan technique (under MW/cm^{-2}-GW/cm^{-2}) [26,28], but close to the reported one using the twin-detector measurement technique (1.41 kW/cm^{-2}) [34]. With the increase of the density, both the saturation intensity and the modulation depth increased. The nonsaturable loss also increased from 11.02% to 12.73%, and to 17.03%.

3. PERFORMANCE OF THE PASSIVELY *Q*-SWITCHED MULTIWAVELENGTH LASER

We applied three as-prepared TI SA samples in the Yb:GAB laser to value their *Q*-switching performance. As presented in Fig. 3, a plano-concave cavity with 18 mm length was used. The pump source was a fiber-coupled continuous wave diode laser at 976 nm with a numerical aperture of 0.22 and a core diameter of 200 μm. The end face of the coupling fiber was focused into the laser crystal with a spot radius of about

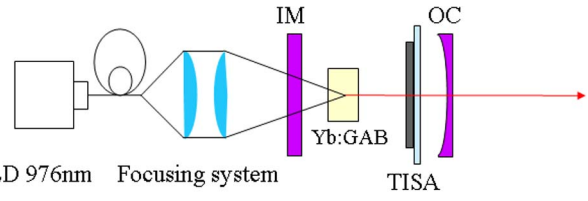

Fig. 3. Schematic experimental setup of the *Q*-switched Yb^{3+}:GAB solid-state laser with TI SA.

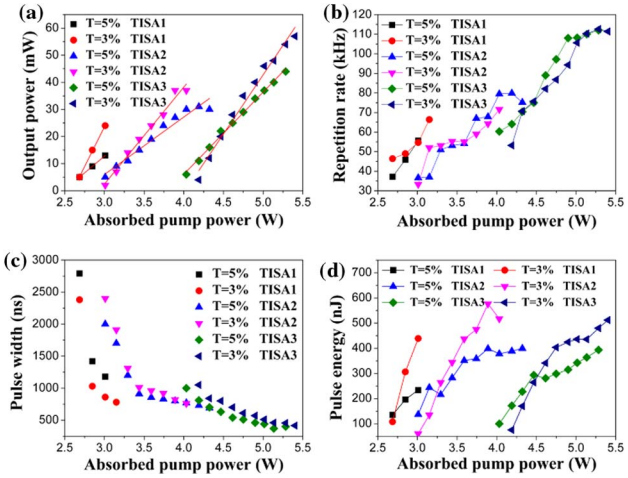

Fig. 4. (a) Average output power as a function of absorbed pump power. (b) Evolution of pulse repetition rate with absorbed pump powers. (c) Evolution of pulsewidth with absorbed pump powers. (d) Evolution of pulse energy with absorbed pump powers.

100 μm. The input mirror (IM) was a plane mirror antireflection (AR) coated at 976 nm and high-reflection (HR) coated at 1020–1080 nm. The output coupler (OC) was a concave mirror with a curvature radius of 75 mm and had a high reflectivity at the pump wavelength. Two OC transmittances of 3% and 5% at 1020–1080 nm were utilized to compare the influence of the transmittance on the laser performance. The laser crystal was an uncoated Yb^{3+}:GAB crystal with dimensions of 3 mm * 3 mm * 2 mm. The crystal was wrapped in foil and mounted in water-cooled Cu blocks. The water temperature was maintained at 20°C.

The quartz substrate coating with TI SA was placed inside the resonant cavity near the output mirror. *Q*-switching operation was realized after optimizing the position and inclination of the plates. Figures 4(a)–4(c) show the recorded average output power, pulse repetition rate, and pulsewidth as a function of absorbed pump power for different combinations of TI SA samples and OCs. Based on the measured average output power and repetition rate, the pulse energy was calculated and shown in Fig. 4(d). The threshold absorbed pump power increased with the density of the TI SA films due to the higher additional optical loss. But the higher coating density shortened the pulse duration and improved the maximum output power thanks to the growth of modulation depth and saturation intensity. Moreover, the threshold and output power increased with the OC transmittance, which is common to a passively *Q*-switched laser. The maximum output powers were obtained to be 24, 37, and 57 mW with a 3% transmission OC for TISA1, TISA2, and TISA3, respectively. The results are comparable to previous reports of *Q*-switched solid-state lasers using TI SAs [32,33]. The corresponding pulsewidths were measured to be 860, 760, and 415 ns respectively, with repetition rates of 54.7, 64.3, and 111.4 kHz. The corresponding pulse energies were calculated to be 438.6, 575.4, and 511.7 nJ, respectively. The drop trend of pulse repetition rate and pulse energy should be attributed to the inevitable thermal effects of the laser crystal under high pump level. The shortest pulse was 370 ns obtained by using 5% OC and TISA3, with 40 mW output power and 110 kHz repetition rate. The 370 ns pulsewidth is much shorter than for the

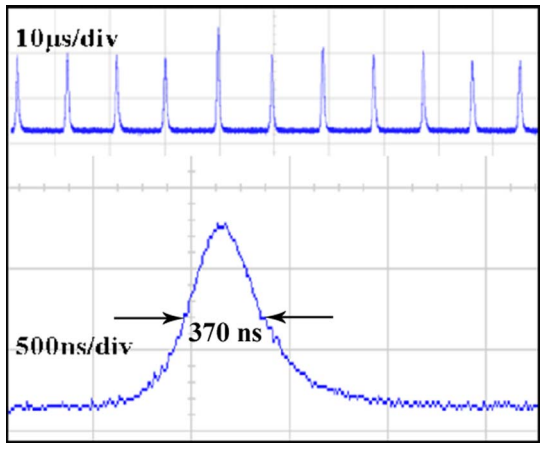

Fig. 5. 370 ns pulse profile and pulse trains.

reported TI-based *Q*-switched solid-state lasers [32–35]. Figure 5 shows the corresponding pulse trains and single pulse profile. When we removed the saturated absorber, no *Q*-switched pulses were observed, even when the output power reached 40 mW. Therefore, the *Q*-switched operation was started and sustained by the saturable absorption effect of the Bi_2Te_3 sheet. Increasing the pump power beyond the ranges in Fig. 4(a) drove the laser to an unstable pulsed regime where cluttered pulse trains appeared due to oversaturation of TI. The *Q*-switched operation was reproducible when returning the pump to the stable range.

The strong crystal field of Yb:GAB leads to a homogeneously broad gain band because of large splitting in the excited and ground states; therefore multiple frequencies can be stimulated equally in laser oscillation. For this reason, the *Q*-switched laser of each combination of OC and TISA operated simultaneously at three wavelengths around 1.04 μm. Figure 6 shows the spectrum of the 370 ns pulses. We can see that this spectrum centers at 1043.7, 1045.3, and 1046.2 nm with FWHM of 0.28, 0.45, and 0.44 nm, respectively. The corresponding frequency differences are 0.44, 0.25, and 0.69 THz, which may be applied to generate terahertz waves with further nonlinear frequency mixing.

For *Q*-switched lasing with a Bi_2Te_3 TI, the modulation depth and saturating intensity related to the density of Bi_2Te_3 film play an important role in the laser operation. A

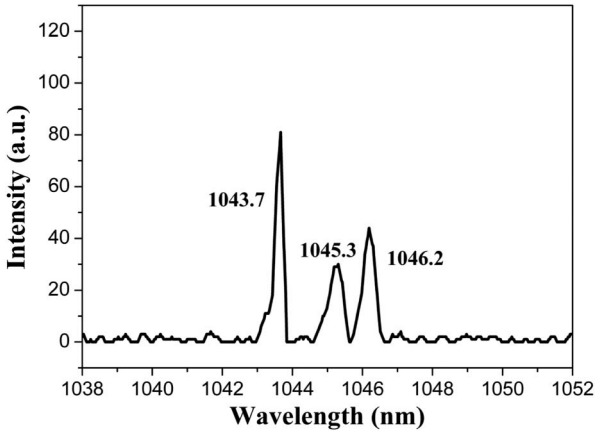

Fig. 6. Laser spectra of the 370 ns pulse laser.

high modulation depth and saturating intensity can shorten the pulse duration and increase the output power. In addition, low OC transmittivity is usually beneficial to the high pulse energy. So the future design of a Bi_2Te_3 TI for the generation of high-energy *Q*-switched pulses should pay much attention to the optimization of the Bi_2Te_3 film density and the OC transmittivity.

4. CONCLUSION

In this paper, we have experimentally presented a tri-wavelength passively *Q*-switched Yb^{3+}:GAB solid-state laser with facile solvothermal synthesized hexagonal Bi_2Te_3 nanosheets as SAs for the first time, to the best of our knowledge. The influence of three TI SA samples with different coating densities on *Q*-switched laser properties was studied. Using the densest TI SA sample and 3% transmission OC, the maximum average output power 57 mW was obtained with pulse energy of 511.7 nJ. The shortest pulsewidth was measured to be 370 ns with 40 mW output power and 110 kHz repetition rate. The 370 ns pulse laser operated at three wavelengths simultaneously at 1043.7, 1045.3, and 1046.2 nm, of which the frequency differences were within the terahertz wave band. This work clearly shows that solvothermal synthesized Bi_2Te_3 is a promising SA for multiwavelength laser operation.

ACKNOWLEDGMENTS

This work is supported by the National Natural Science Foundation of China (50902129, 51472240, 61078076, 91122033, and 11304313), the Knowledge Innovation Program of Chinese Academy of Sciences (KJCX2-EW-H03), and the Key Laboratory of Functional Crystal Materials and Device (Shandong University, Ministry of Education).

REFERENCES

1. R. W. Farley and P. D. Dao, "Development of an intracavity summed multiple-wavelength Nd:YAG laser for a rugged solid-state sodium lidar system," Appl. Opt. **34**, 4269–4273 (1995).
2. S. N. Son, J. J. Song, J. U. Kang, and C. S. Kim, "Simultaneous second harmonic generation of multiple wavelength laser outputs for medical sensing," Sensors **11**, 6125–6130 (2011).
3. G. Gulsen, B. Xiong, O. Birgul, and O. Nalcioglu, "Design and implementation of a multifrequency near-infrared diffuse optical tomography system," J. Biomed. Opt. **11**, 014020 (2006).
4. D. G. Abdelsalam, R. Magnusson, and D. Kim, "Single-shot, dual-wavelength digital holography based on polarizing separation," Appl. Opt. **50**, 3360–3368 (2011).
5. F. Zernike, Jr. and P. R. Bermanf, "Generation of far infrared as a difference frequency," Phys. Rev. Lett. **15**, 999–1001 (1965).
6. J. E. Schaar, K. L. Vodopyanov, and M. M. Fejer, "Intracavity terahertz-wave generation in a synchronously pumped optical parametric oscillator using quasi-phase-matched GaAs," Opt. Lett. **32**, 1284–1286 (2007).
7. Y. Q. Du, B. Q. Yao, X. M. Duan, Z. Cui, Y. Ding, Y. L. Ju, and Z. C. Shen, "Cr:ZnS saturable absorber passively *Q*-switched Tm, Ho:$GdVO_4$ laser," Opt. Express **21**, 26506–26512 (2013).
8. A. Brenier, C. Y. Tu, Z. J. Zhu, and J. F. Li, "Diode pumped passive *Q* switching of Yb^{3+}-doped $GdAl_3(BO_3)_4$ nonlinear laser crystal," Appl. Phys. Lett. **90**, 071103 (2007).
9. S. Y. Zhang, H. T. Huang, L. Xu, M. J. Wang, F. Chen, J. Q. Xu, J. L. He, and B. Zhao, "Continuous wave and passively *Q*-switched Nd: $Lu_xY_{1-x}VO_4$ laser at 1.34 μm with V^{3+}:YAG as the saturable absorber," Opt. Express **19**, 1830–1835 (2011).
10. A. Agnesi, A. Guandalini, G. Reali, J. K. Jabczynski, K. Kopczynski, and Z. Mierczyk, "Diode pumped Nd:YVO_4 laser at 1.34 μm *Q*-switched and mode locked by a V:YAG saturable absorber," Opt. Commun. **194**, 429–433 (2001).
11. H. Qi, X. Hou, Y. Li, Y. Sun, H. Zhang, and J. Wang, "Co^{2+}:$LaMgAl_{11}O_{19}$ saturable absorber *Q*-switch for a flash lamp pumped 1.54 μm Er: glass laser," Opt. Express **15**, 3195–3200 (2007).
12. J. Hou, L. H. Zheng, J. L. He, J. Xu, B. T. Zhang, Z. W. Wang, F. Lou, R. H. Wang, and X. M. Liu, "A tri-wavelength synchronous mode-locked Nd:SYSO laser with a semiconductor saturable absorber mirror," Laser Phys. Lett. **11**, 035803 (2014).
13. B. Dannecker, X. Délen, K. S. Wentsch, B. Weichelt, C. Hönninger, A. Voss, M. A. Ahmed, and T. Graf, "Passively mode-locked Yb:CaF_2 thin-disk laser," Opt. Express **22**, 22278–22284 (2014).
14. A. Klenner, M. Golling, and U. Keller, "High peak power gigahertz Yb:CALGO laser," Opt. Express **22**, 11884–11891 (2014).
15. K. H. Lin, J. J. Kang, H. H. Wu, C. K. Lee, and G. R. Lin, "Manipulation of operation states by polarization control in an erbium-doped fiber laser with a hybrid saturable absorber," Opt. Express **17**, 4806–4814 (2009).
16. X. L. Li, J. L. Xu, Y. Z. Wu, J. L. He, and X. P. Hao, "Large energy laser pulses with high repetition rate by graphene *Q*-switched solid-state laser," Opt. Express **19**, 9950–9955 (2011).
17. J. L. Xu, X. L. Li, J. L. He, X. P. Hao, Y. Yang, Y. Z. Wu, S. D. Liu, and B. T. Zhang, "Efficient graphene *Q* switching and mode locking of 1.34 μm neodymium lasers," Opt. Lett. **37**, 2652–2654 (2012).
18. T. L. Feng, S. Z. Zhao, K. J. Yang, G. Q. Li, D. C. Li, J. Zhao, W. C. Qiao, J. Hou, Y. Yang, J. L. He, L. H. Zheng, Q. G. Wang, X. D. Xu, L. B. Su, and J. Xu, "Diode-pumped continuous wave tunable and graphene *Q*-switched Tm:LSO lasers," Opt. Express **21**, 24665–24673 (2013).
19. J. L. Xu, X. L. Li, Y. Z. Wu, X. P. Hao, J. L. He, and K. J. Yang, "Graphene saturable absorber mirror for ultra-fast-pulse solid-state laser," Opt. Lett. **36**, 1948–1950 (2011).
20. J. L. Xu, X. L. Li, J. L. He, X. P. Hao, Y. Z. Wu, Y. Yang, and K. J. Yang, "Performance of large-area few-layer graphene saturable absorber in femtosecond bulk laser," Appl. Phys. Lett. **99**, 261107 (2011).
21. H. Zhang, C. X. Liu, X. L. Qi, X. Dai, Z. Fang, and S. C. Zhang, "Topological insulators in Bi_2Se_3, Bi_2Te_3, Sb_2Te_3 with a single Dirac cone on the surface," Nat. Phys. **5**, 438–442 (2009).
22. H. Yu, H. Zhang, Y. Wang, C. Zhao, B. Wang, S. Wen, H. Zhang, and J. Wang, "Topological insulator as an optical modulator for pulsed solid-state lasers," Laser Photon. Rev. **7**, L77–L83 (2013).
23. S. Q. Chen, C. J. Zhao, Y. Li, H. H. Huang, S. B. Lu, H. Zhang, and S. C. Wen, "Broadband optical and microwave nonlinear response in topological insulator," Opt. Mater. Express **4**, 587–596 (2014).
24. F. Bernard, H. Zhang, S. P. Gorza, and P. Emplit, "Towards mode-locked fiber laser using topological insulators," in *Advanced Photonics Congress*, OSA Technical Digest (online) (Optical Society of America, 2012), paper NTh1A.5.
25. C. J. Zhao, H. Zhang, X. Qi, Y. Chen, Z. T. Wang, S. C. Wen, and D. Y. Tang, "Ultra-short pulse generation by a topological insulator based saturable absorber," Appl. Phys. Lett. **101**, 211106 (2012).
26. Z. Q. Luo, Y. Z. Huang, J. Weng, H. H. Cheng, Z. P. Lin, B. Xu, Z. P. Cai, and H. Y. Xu, "1.06 μm *Q*-switched ytterbium-doped fiber laser using few-layer topological insulator Bi_2Se_3 as a saturable absorber," Opt. Express **21**, 29516–29522 (2013).
27. M. Jung, J. Lee, J. H. Koo, J. Park, Y. W. Song, K. Lee, S. Lee, and J. H. Lee, "A femtosecond pulse fiber laser at 1935 nm using a bulk-structured Bi_2Te_3 topological insulator," Opt. Express **22**, 7865–7874 (2014).
28. M. Liu, N. Zhao, H. Liu, X. W. Zheng, A. P. Luo, Z. C. Luo, W. C. Xu, C. J. Zhao, H. Zhang, and S. C. Wen, "Dual-wavelength harmonically mode-locked fiber laser with topological insulator saturable absorber," IEEE Photon. Technol. Lett. **26**, 983–986 (2014).
29. J. Sotor, G. Sobon, K. Grodecki, and K. M. Abramski, "Mode-locked erbium-doped fiber laser based on evanescent field interaction with Sb_2Te_3 topological insulator," Appl. Phys. Lett. **104**, 251112 (2014).
30. C. J. Zhao, Y. H. Zou, Y. Chen, Z. T. Wang, S. B. Lu, H. Zhang, S. C. Wen, and D. Y. Tang, "Wavelength-tunable picosecond soliton

fiber laser with topological insulator: Bi_2Se_3 as a mode locker," Opt. Express **20**, 27888–27895 (2012).
31. Y. H. Lin, C. Y. Yang, S. F. Lin, W. H. Tseng, Q. Bao, C. Wu, and G. R. Lin, "Soliton compression of the erbium-doped fiber laser weakly started mode-locking by nanoscale p-type Bi_2Te_3 topological insulator particles," Laser Phys. Lett. **11**, 055107 (2014).
32. H. H. Yu, H. Zhang, Y. C. Wang, C. J. Zhao, B. L. Wang, S. C. Wen, H. J. Zhang, and J. Y. Wang, "Topological insulator as an optical modulator for pulsed solid-state lasers," Laser Photon. Rev. **7**, L77–L83 (2013).
33. B. L. Wang, H. H. Yu, H. Zhang, C. J. Zhao, S. C. Wen, H. J. Zhang, and J. Y. Wang, "Topological insulator simultaneously *Q*-switched dual-wavelength Nd:Lu_2O_3 laser," IEEE Photon. J. **6**, 1501007 (2014).
34. P. H. Tang, X. Q. Zhang, C. J. Zhao, Y. Wang, H. Zhang, D. Y. Shen, S. C. Wen, D. Y. Tang, and D. Y. Fan, "Topological insulator: Bi_2Te_3 saturable absorber for the passive *Q*-switching operation of an in-band pumped 1645-nm Er:YAG ceramic laser," IEEE Photon. J. **5**, 1500707 (2013).
35. M. T. Hu, J. H. Lin, J. R. Tian, Z. Y. Dou, and Y. R. Song, "Generation of *Q*-switched pulse by Bi_2Se_3 topological insulator in Yb:KGW laser," Laser Phys. Lett. **11**, 115806 (2014).
36. Z. Zhu, J. Li, B. Alain, G. Jia, Z. You, X. Lu, B. Wu, and C. Tu, "Growth, spectroscopic and laser properties of Yb^{3+}-doped $GdAl_3(BO_3)_4$ crystal: a candidate for infrared laser crystal," Appl. Phys. B **86**, 71–75 (2007).
37. A. Brenier, C. Tu, Z. Zhu, and J. Li, "Optical bifurcated fiber diode-pumping for two-wavelength laser operation with the Yb^{3+}-doped $GdAl_3(BO_3)_4$ birefringent crystal," Appl. Phys. B **98**, 401–406 (2010).
38. Y. Zhang, L. P. Hu, T. J. Zhu, J. Xie, and X. B. Zhao, "High yield Bi_2Te_3 single crystal nanosheets with uniform morphology via a solvothermal synthesis," Cryst. Growth Des. **13**, 645–651 (2013).
39. Q. L. Bao, H. Zhang, Y. Wang, Z. H. Ni, Y. L. Yan, Z. X. Shen, K. P. Loh, and D. Y. Tang, "Atomic-layer graphene as a saturable absorber for ultrafast pulsed lasers," Adv. Funct. Mater. **19**, 3077–3083 (2009).